Composite Structures 249 (2020) 112486

Contents lists available at ScienceDirect

Composite Structures

journal homepage: www.elsevier.com/locate/compstruct

A new hyperbolic-polynomial higher-order elasticity theory for mechanics of thick FGM beams with imperfection in the material composition

Mohammad Malikan [a], Victor A. Eremeyev [a,b,*]

[a] Department of Mechanics of Materials and Structures, Faculty of Civil and Environmental Engineering, Gdansk University of Technology, 80-233 Gdansk, Poland
[b] Research Institute for Mechanics, Nizhniy Novgorod Lobachevski State University, Russia

ARTICLE INFO

Keywords:
Novel elasticity theory
FGM beam
Imperfection
Galerkin analytical method
Different edge conditions

ABSTRACT

A drawback to the material composition of thick functionally graded materials (FGM) beams is checked out in this research in conjunction with a novel hyperbolic-polynomial higher-order elasticity beam theory (HPET). The proposed beam model consists of a novel shape function for the distribution of shear stress deformation in the transverse coordinate. The beam theory also incorporates the stretching effect to present an indirect effect of thickness variations. As a result of compounding the proposed beam model in linear Lagrangian strains and variational of energy, the system of equations is obtained. The Galerkin method is here expanded for several edge conditions to obtain elastic critical buckling values. First, the importance of the higher-order beam theory, as well as stretching effect, is assessed in assorted tabulated comparisons. Next, with validations based on the existing and open literature, the proposed shape function is evaluated to consider the desired accuracy. Some comparative graphs by means of well-known shape functions are plotted. These comparisons reveal a very good compliance. In the final section of the paper, based on an inappropriate mixture of the SUS304 and Si_3C_4 as the first type of FGM beam (Beam-I) and, Al and Al_2O_3 as the second type (Beam-II), the results are pictured while the beam is kept in four states, clamped–clamped (C–C), pinned–pinned (S–S), clamped-pinned (C–S) and in particular cantilever (C–F). We found that the defect impresses markedly an FGM beam with boundary conditions with lower degrees of freedom.

1. Introduction

1.1. FGMs

Functionally graded materials (FGMs) are those whose mechanical properties change gently and continuously from one surface to another according to a given function. These materials are built up by composing of ceramic and metal or aluminum and alumina powders, etc. The common sort of these materials may be a mixture of ceramics and metals attachments. The main merit of using such the material is that it can withstand severe situations such as environments with very high temperature and high temperature's difference. For example, thermal coating on blades of gas turbines and heat shields of spacecraft can be some great promises of their applications. Besides, this kind of composite structure is resistant to corrosion and wear, and has high resistance to fracture. In relation to this, some instances can be brought up such as the chemical tanks and high abrasion environments due to its specificity [1–5].

1.2. Beams

Beams, as one of the most vital engineering components, have always been of interest to researchers. The instability of beams results in buckling under a static in-plane load which due to the large deformation of the structure in this case, the efficiency of the beam will be vastly diminished. Assorted methods for analyzing beams have been presented so far. The method of analyzing the behavior of a beam using the theory of three-dimensional elasticity, although a basic and precise method, is complicated and difficult because of the three-dimensional analysis of the beam. To reduce these complexities, and assuming that the thickness of the beams is small to a great extent compared to other dimensions like length, assumptions called beam theories are presented. The simplest theory in beam analysis is

* Corresponding author at: Department of Mechanics of Materials and Structures, Faculty of Civil and Environmental Engineering, Gdansk University of Technology, 80-233 Gdansk, Poland.
E-mail addresses: victor.eremeev@pg.edu.pl, eremeyev.victor@gmail.com (V.A. Eremeyev).

https://doi.org/10.1016/j.compstruct.2020.112486
Received 18 March 2020; Revised 10 May 2020; Accepted 14 May 2020
Available online 31 May 2020
0263-8223/

Nomenclature

z	Thickness coordinate	E_1	Ceramic or Alumina Young's modulus
$\nu(z)$	FGM Poisson's ratio	E_2	Metal or Aluminium Young's modulus
$E(z)$	FGM Young's modulus	w_b	Transverse deflection of the beam' nodes
w_z	Thickness stretching	w_s	Shear deflection of the beam' nodes
Π_W	Work performed by external loads	$f(z)$	Shape function of shear deformation
ν_1	Ceramic or Alumina Poisson's ratio	$g(z)$	Shape function of stretching effect
ν_2	Metal or Aluminium Poisson's ratio	k	Volume fraction, Power-law index
h	Thickness of the beam	$G(z)$	Shear modulus of the beam material
L	Length of the beam	M_{xx}	Moment stress resultant around × axis
ε_{xx}	Axial strain	N_{xx}	Axial in-plane stress resultant
γ_{xz}	Shear strain in x-z plane	Q_{xz}	Shear stress resultants in x-z plane
ε_{zz}	Transverse strain	X_m	Weight function to satisfy boundary conditions
σ_{xx}	Axial stress	a	To define the imperfection in Ceramic section
τ_{xz}	Shear stress	b	To define the imperfection in Metal section
σ_{zz}	Transverse stress	N^0_{xx}	In-plane static compression applied at the both ends of the beam
Π_b	Strain energy	R_{xx}, R_{zz}	Higher-order and thickness stretching stress resultants
m	mode number	U_m,W_{bm},W_{sm}	Unknown variables for axial, transverse, and shear deflections
u_1	Axial displacement of the beam' nodes	W_{zm}	Stretching effect
u_3	Transverse displacement of the beam' nodes		
u	In-plane displacement of the beam' nodes along x		

Euler-Bernoulli (EB) beam theory. The EB hypothesis corresponds to the thin beams and does not consider the effect of shear and transverse deformation along the thickness. In order to lessen the error in the analysis of relatively thick beams, another theory known as shear deformation theory was introduced [6]. In this theory, the effect of shear deformation on the thickness is considered, however it confronts with an error for which there is need to a shear correction factor. The most common higher-order shear deformation theory can be the third-order shear deformation theory raised by Reddy [7]. Although beam shear deformation theories have yielded good results in analysis of comparatively thick beams, they are far from accurate answers yet because of the neglect of transverse strains and stretching effects across the thickness. To fix this problem and maximize the accuracy, quasi-3D elasticity came [8–12]. However, these theories work well only for isotropic thick materials and cannot be a general quasi-3d elasticity model appropriate for all materials such as laminated composites. This theory complements previous theories and considers both the effects of shear and transverse deformation along the thickness in the form of a higher-order beam theory.

1.3. Literature review

Due to the outstanding and overriding applications of FGM structures, it is important to study the conditions of their failure and defective. In the past, due to being unknown the buckling phenomenon, yield resistance was considered as a key indicator in most designs. However, as the studies have begun to recognize this important criterion, the buckling phenomenon has been considered as the main criterion in design considerations. The buckling phenomenon occurs when most of the strain energy stored in the membrane is capable of converting the bending energy necessary for large deformations, which can lead to catastrophic damage. Buckling in a member depends on factors such as loading, geometry and material. The theoretical works pertinent to the buckling of FGM beams are dependent on a variety of researchers. Kiani and Eslami [13] performed analysis of FGM beams subject to thermal stability on the basis of EB beam approach as well as power-law distribution. They estimated three types of distribution for temperature, namely linear, nonlinear and uniform temperature rise. Different edge conditions also were considered as pinned–pinned and clamped-pinned ones. Ultimately, the governed equations were solved based on an exact solution. Wattanasakulpong et al. [14] based on the power-law, inspected natural frequencies and thermal critical stability loads for an FGM beam using a refined third-order shear deformation theory (TSDT). The eigen-frequency analysis was adopted by Ritz method. Fallah and Aghdam [15] attended the nonlinear response for a EB-FGM beam in an instability and vibrating limit to study thermo-elasticity problem. The beam was installed on a nonlinear elastic matrix, and several end conditions as well. Ma and Lee [16] through a first-order shear deformation theory (FSDT), investigated nonlinearity into behavior of a pivot-pivot FGM beam involving shear deformations under in-plane thermal loading based on the exact solution technique. Rahimi et al. [17] studied natural frequencies and post-critical stability for an FGM beam containing shear deformations on the basis of FSDT. The beam was implemented at both ends by pinned–pinned, fixed–fixed, and fixed-pinned conditions. Esfahani et al. [18] discussed a temperature-dependent composite beam subjected to nonlinear thermal buckling loads. FSDT was employed while the system included a nonlinear elastic substrate. The outcomes were given in fixed and hinged edge conditions utilizing generalized differential quadrature method (GDQM). Viola et al. [19] formulated and computed the free vibration conditions of doubly-curved composite panels and shells in the framework of a higher-order elasticity theory. Their problem was solved with respect to the GDQ method and validated by FSDT and commercial computer programs e.g. ABAQUS as well. In another work, Viola et al. [20] on the basis of a higher-order elasticity theory and GDQ technique surveyed static response of a perfect doubly-curved composite panels and shells. They investigated six groups of panels and shells such as spherical and cylindrical panels, rectangular and annular plates, in particular an elliptic paraboloid and a catenoidal shell. Tornabene et al. [21] proposed an equivalent single-layer model for laminated composite structures in order to study free vibrations of the modeled single-layer shell/panel. Their consideration also covered the zig-zag and stretching effects for the material. The GDQ and generalized integral quadrature (GIQ) approach gave solutions for the problem. Results of commercial codes and other literature approved their formulation. Vo et al. [22] addressed stability and vibration of a composite sandwich beam regarding a modified higher-order shear deformation theory (HSDT) by finite element technique. Tornabene et al. [23] applied a radial basis function (RBF) technique in order to compute natural frequencies of a composite doubly-curved shell/panel in the framework of an equivalent single-layer model. The reliability and stability of the

methodology were confirmed by comparison the results with FEM and GDQ. Shen and Wang [24] nonlinearly considered large deflections, post-stability situation and vibration amplitude for an FGM beam incorporating shear deformations whilst the beam was embedded into an environment with temperature differential and also a polymer foundation. Tornabene et al. [25] presented a general higher-order approach in order to study natural frequencies of doubly-curved composite structures such as laminated shells. To calculate the tabular and pictorial results, they employed an advanced version of GDQ, namely local GDQ (LGDQ). The merit of this method in comparison with the previous one, however, was the necessity to lower number of grid points by keeping the accuracy. Nguyen et al. [26] focused on a new HSDT to analyze a sandwich composite beam exposed in stability and eigen-frequency conditions. The numerical outputs were captured on the basis of the method of Lagrange multiplier for boundary conditions of fixed–fixed, pinned–pinned and their mixture. Tufeksi et al. [27] examined circular cross-sectional FGM beams with FSDT under in-plane stability condition by the help of exact solution technique. Chen et al. [28] evaluated porosity into an FGM beam and devoted static analysis based on buckling and bending of FSDT beam and solved the harvested characteristic relation by employing Ritz method for some cases of end conditions, namely hinged, fixed, free and their combinations. Simsek [29] presented functionality into two directions for a FSDT-FGM beam comprising several boundary conditions on the basis of Ritz method. Huang et al. [30] based on the FSDT, analyzed axial stability of a FSDT-FGM beam by assuming inhomogeneity into direction of length. By the basis on numerical solutions, a variety of end supports were estimated as free, fixed, hinged and particularly guided ones. She et al. [31] inspected a HSDT to study post-critical and thermal stability of an FGM beam. They captured the results using a two-step perturbation technique. Kahya and Turan [32] acquired a finite element model for a composite beam under buckling and vibration states. The FSDT and Lagrange equation aided to achieve the constitutive equations. A study on stability and vibrations of a double system of composite beam based on FSDT bridged on Winkler-Pasternak medium has been performed by Deng et al. [33]. To shorten the review of the broad number of published works, further significant research can be seen by [34–66], and elsewhere.

1.4. Imperfection

As assessments by the published researches make clear, all the literature about FGM were often done on the basis of theoretical assumptions of a perfect structure for mechanical properties of FGMs. Undoubtedly, it is arduous to explore the exact gradation in the FGMs as it needs an experimental control. However, controlling of almost all the produced parts made of FGMs may be not cost-effective, which leads to some imperfect products. On the other side, todays, several strong techniques have been being employed to manufacture FGMs, but a few of them may produce constituents of these prestigious materials excellently without defects [67]. Thus, devoid of a defect for attaining a fluently and continuity varying gradation and a perfect structure may be impossible. Although in this paper we assume a theoretical model for FGMs as well, it is based on the imperfect FGMs. Taking a look at literature, one can find the [68] in which the material properties of FGMs were assayed with an imperfection. However, the research was based on the converting FGMs into laminated composites to make a path to study the imperfection. Contrary to this reference, in the present research, we try to put the drawback to the material composition on the basis of the functionality gradation of power-law distribution.

1.5. Briefly review of present paper

In the present study, a new shear deformation function is presented for the stability analysis of thick and very thick rectangular beams made of functionally graded materials. Taking the change in thickness as a function of the x dimension, we transform the problem into a higher-order elasticity problem. The material properties are considered unaltered in accordance with the thickness axis. In the perfect form of functionally graded materials, the properties of the material change continuously and gradually according to the various patterns such as exponential, power and sigmoid law [55]. In this paper, we attempt to bring the perfect form of functionally graded materials into some imperfections in the material composition. Indeed, it is unlikely that a calibrated material to comply with exactly the pattern law. Since there can be potential errors in the blending process, so in this study we have considered two functional cases of imperfect calibration based on the power-law in order to find out what the difference in their results will be if they do not exactly comply with the power-law. Also, due to the importance of the Poisson's ratio of graded materials, its value along the thickness of the member is considered as a function of both materials. In the first step, in order to investigate the stability behavior of the member, the governing equation for buckling of the rectangular beam is obtained using a combination of the principle of minimum potential energy and the higher-order elasticity theory. As a result, the approximate form of the deformation of the beam is obtained as an ordinary differential equation and by imposing the edge conditions of the beam, and by use of the eigenvalue solver method, the critical buckling loads are attained. At the validation, numerical results of stability analysis are compared with prestigious references and finite element (FE) solution software. An overview is performed on the most well-known shear deformation functions provided hitherto by other researchers. Numerical results are presented for members made of functionally graded materials and the influences of cross-sectional area, material power-law, and type of edge support on critical buckling load are investigated part by part. In all comparison tables, the efficiency, accuracy and reliability of the presented function have been approved.

The novelty of the current work can be written as

- A new shape function based on the hyperbolic-polynomial terms is guessed to present a new higher-order elasticity analysis.
- An imperfection in the material composition is here considered on the basis of two patterns.
- Four disparate boundary conditions are investigated by an analytical solution method, presenting and developing a new admissible function for free edges.

Eventually, this research can make a bridge for researchers to commence considering other forms of defect in the material composition of FGMs.

2. Mathematical model

An axially compressed rectangular FGM beam is taken into consideration with length L, thickness h and width t in a rectangular coordinate system (Fig. 1).

As far as each mathematic function has its own specific behavior, in our work, the aim is to find a new mathematic function for shear deformation across the thickness of the thick FGM beam. The combination of a hyperbolic function with a polynomial one was derived as a new framework in the analysis of thick beams/plates. Here, the transverse displacement contains three parts, namely bending (w_b), shear (w_s) and an extra one ($g(z)w_z(x)$). The effect of stretching in the thickness is evaluated according to the extra part which itself is function of the x and z-axes. Thus, the present higher-order elasticity theory is here adopted as

$$u_1(x,z) = u(x) - z\frac{dw_b(x)}{dx} - f(z)\frac{dw_s(x)}{dx}u_3(x,z) = w_b(x) + w_s(x) + g(z)w_z(x) \quad (1a\text{-}b)$$

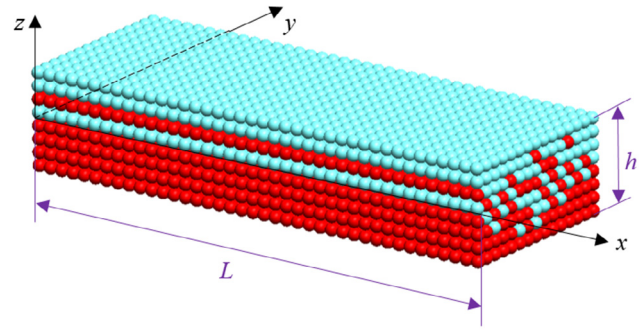

Fig. 1. An FGM beam illustrated schematically.

in which

$$f(z)=\tanh\left(z/h-(z/h)^3-r(z/h)^5\right);\ [r=0.8]$$

$$g(z)=\left(1-f'(z)\right)$$

where the shape function follows a comma which means differentiation of the variable. To introduce the taken imperfect, first, the power-law material gradation can be presented as below [69–71]

$$E(z)=E_2+(E_1-E_2)\left(\frac{1}{2}+\frac{z}{h}\right)^k \tag{2a}$$

$$\nu(z)=\nu_2+(\nu_1-\nu_2)\left(\frac{1}{2}+\frac{z}{h}\right)^k \tag{2b}$$

The distribution of elasticity modulus respecting Eq. (2a) would give the Fig. 2 in a perfect structure of FGMs.

The imperfection in the material composition of FGMs can, however, be observed in dissimilar cases, this research is concerned with the cases drawn by Figs. 3a and 3b. Conforming to this figures we can reveal the Table 1 in which two cases are totally shown. In the first case, we assume that the pure ceramic section consists of a part of thickness and after the range the gent composition will start. As a matter of fact, in the imperfect cases, we have a layer of a pure ceramic or metal and thereafter the power-law composition will appear. This taken range here is displayed for the first case by a and the latter case by b for which we assume a notable section of thickness is graded with pure metal only. These are just topmost and bottommost layer in a perfect FGM for pure ceramic and metal zones.

As we are studying a linear stability problem, one can get the linear Lagrangian strain as

$$\varepsilon_{ij}=\frac{1}{2}\left(\frac{\partial u_i}{\partial x_j}+\frac{\partial u_j}{\partial x_i}\right) \tag{3}$$

Imposing Eq. (3) on Eq. (1), one can obtain the strain–displacement relations as

$$\varepsilon_{xx}=\frac{du}{dx}-z\frac{d^2w_b}{dx^2}-f(z)\frac{d^2w_s}{dx^2} \tag{4a}$$

$$\varepsilon_{xz}=g(z)\left(\frac{dw_s}{dx}+\frac{dw_z}{dx}\right) \tag{4b}$$

$$\varepsilon_{zz}=g'(z)w_z \tag{4c}$$

If we assume the Lagrangian in a variated state, thus

$$\delta(\Pi_b+\Pi_W)=0 \tag{5}$$

The strain energy can be demonstrated as

$$\Pi_b=\int_V(\sigma_{xx}\varepsilon_{xx}+\tau_{xz}\gamma_{xz}+\sigma_{zz}\varepsilon_{zz})dV \tag{6}$$

in which

$$\begin{bmatrix}\sigma_{xx}\\ \sigma_{zz}\\ \tau_{xz}\end{bmatrix}=\begin{bmatrix}C_{11}&C_{12}&0\\ C_{12}&C_{22}&0\\ 0&0&C_{33}\end{bmatrix}\begin{bmatrix}\varepsilon_{xx}\\ \varepsilon_{zz}\\ \gamma_{xz}\end{bmatrix} \tag{7}$$

where the stiffness elasticity matrix can be defined as

$C_{11}=\frac{(1-\nu(z))E(z)}{(1-2\nu(z))(1+\nu(z))}$, $C_{22}=C_{11}$,

$C_{12}=\frac{\nu(z)E(z)}{(1-2\nu(z))(1+\nu(z))}$, $C_{33}=G(z)=\frac{E(z)}{2(1+\nu(z))}$

Eq. (6) based on Eq. (7) can be expanded as

$$\delta\Pi_b=\int_0^L\left[N_{xx}\frac{d\delta u}{dx}-M_{xx}\frac{d^2\delta w_b}{dx^2}-R_{xx}\frac{d^2\delta w_s}{dx^2}+Q_{xz}\left(\frac{d\delta w_s}{dx}+\frac{d\delta w_z}{dx}\right)+R_{zz}\delta w_z\right]dx \tag{8}$$

in which

$$N_{xx},M_{xx},R_{xx}=\int_{-h/2}^{h/2}\sigma_{xx}(1,z,f(z))dz \tag{9a-c}$$

$$Q_{xz}=\int_{-h/2}^{h/2}\sigma_{xz}g(z)dz \tag{9d}$$

$$R_{zz}=\int_{-h/2}^{h/2}\sigma_{zz}g'(z)dz \tag{9e}$$

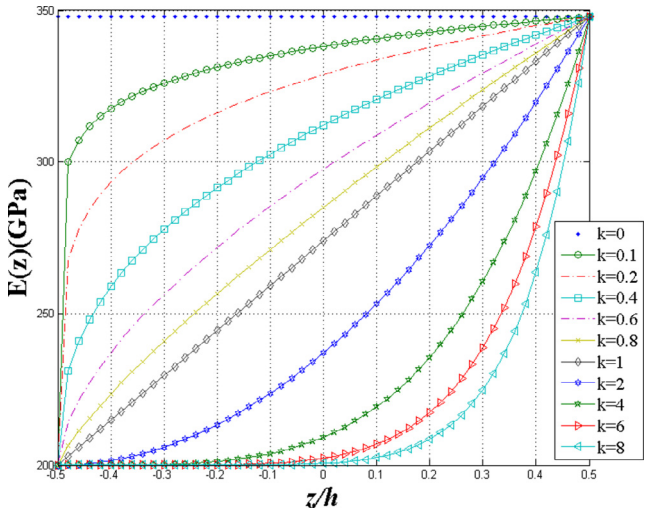

Fig. 2. Variation of the Young's modulus based on the power-law for a perfect FGM beam-I.

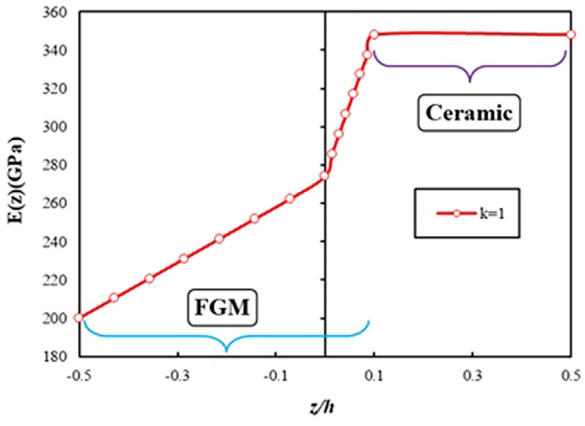

Fig. 3a. Variation of the Young's modulus for an imperfect FGM beam-I (Case I, $a=0.1h$).

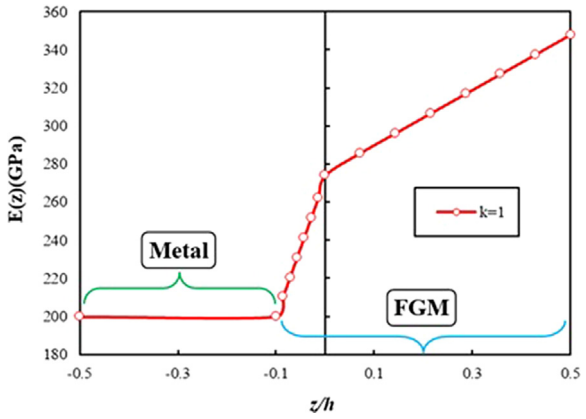

Fig. 3b. Variation of the Young's modulus for an imperfect FGM beam-I (Case II, $b = 0.1h$).

where the expressed stress resultants can be extended as below

$$N_{xx} = A_{11}\frac{du}{dx} - A_{12}\frac{d^2w_b}{dx^2} - A_{33}\frac{d^2w_s}{dx^2} + D_{33}w_z \tag{10a}$$

$$M_{xx} = A_{12}\frac{du}{dx} - D_{11}\frac{d^2w_b}{dx^2} - D_{12}\frac{d^2w_s}{dx^2} + D_{44}w_z \tag{10b}$$

$$R_{xx} = A_{33}\frac{du}{dx} - D_{12}\frac{d^2w_b}{dx^2} - D_{22}\frac{d^2w_s}{dx^2} + D_{55}w_z \tag{10c}$$

$$Q_{xz} = A_{44}\left(\frac{dw_s}{dx} + \frac{dw_z}{dx}\right) \tag{10d}$$

$$R_{zz} = A_{66}\frac{du}{dx} - A_{77}\frac{d^2w_b}{dx^2} - A_{88}\frac{d^2w_s}{dx^2} + A_{55}w_z \tag{10e}$$

in which we define

$$A_{11}, A_{12}, A_{33}, D_{11}, D_{12}, D_{22} = \int_{-h/2}^{h/2} C_{11}\left(1, z, f(z), z^2, zf(z), f^2(z)\right)dz$$

$$D_{33}, D_{44}, D_{55} = \int_{-h/2}^{h/2} C_{12}(g'(z), zg'(z), f(z)g'(z))dz$$

$$A_{44} = \int_{-h/2}^{h/2} C_{33}g^2(z)dz,\ A_{55} = \int_{-h/2}^{h/2} C_{22}g'^2(z)dz,$$
$$A_{66}, A_{77}, A_{88} = \int_{-h/2}^{h/2} C_{12}(1, z, f(z))dz$$

Consider an in-plane axially compressive load gradually applied at both ends of the beam does a work as

$$\Pi_W = \frac{1}{2}\int_0^L N_{xx}^0\left(\frac{dw_b}{dx} + \frac{dw_s}{dx}\right)^2 dx \tag{11}$$

By variation the above relation, one can explore

$$\delta\Pi_W = \int_0^L N_{xx}^0\left[\frac{d\delta w_b}{dx}\frac{dw_b}{dx} + \frac{d\delta w_s}{dx}\frac{dw_s}{dx} + \delta\left(\frac{dw_b}{dx}\frac{dw_s}{dx}\right)\right]dx \tag{12}$$

Gaining the equations which govern a static response of the FGM beam requires to unpack Eq. (5) as below

$$\delta u = 0: \ \frac{dN_{xx}}{dx} = 0 \tag{13a}$$

$$\delta w_b = 0: \ \frac{d^2M_{xx}}{dx^2} + N_{xx}^0\left(\frac{d^2w_b}{dx^2} + \frac{d^2w_s}{dx^2}\right) = 0 \tag{13b}$$

$$\delta w_s = 0: \ \frac{dQ_{xz}}{dx} + \frac{d^2R_{xx}}{dx^2} + N_{xx}^0\left(\frac{d^2w_b}{dx^2} + \frac{d^2w_s}{dx^2}\right) = 0 \tag{13c}$$

$$\delta w_z = 0: \ \frac{dQ_{xz}}{dx} - R_{zz} = 0 \tag{13d}$$

Thereby, in terms of displacements, by means of Eq. (10), one can re-write the above equations as

$$A_{11}\frac{d^2u}{dx^2} - A_{12}\frac{d^3w_b}{dx^3} - A_{33}\frac{d^3w_s}{dx^3} + D_{33}\frac{dw_z}{dx} = 0 \tag{14a}$$

$$A_{12}\frac{d^3u}{dx^3} - D_{11}\frac{d^4w_b}{dx^4} - D_{12}\frac{d^4w_s}{dx^4} + D_{44}\frac{d^2w_z}{dx^2} + N_{xx}^0\left(\frac{d^2w_b}{dx^2} + \frac{d^2w_s}{dx^2}\right) = 0 \tag{14b}$$

Table 1
Patterns of the FGM beam-I considered here, Perfect (a), Imperfect (Case I (b), Case II (c)).

Ceramic Metal	
Ceramic-rich	Perfect FGMs $E(z) = E_2 + (E_1 - E_2)\left(\frac{1}{2} + \frac{z}{h}\right)^k;$ $-0.5h \leqslant z \leqslant 0.5h$
Metal-rich	Imperfect FGMs (Case-I): $E_1(z) = E_2 + (E_1 - E_2)\left(\frac{1}{2} + \frac{z}{h}\right)^k;\ -0.5h \leqslant z \leqslant 0$ $E_2(z) = E_2 + (E_1 - E_2)\left(\frac{1}{2} + \frac{z}{h}\right)^k;\ 0 \leqslant z \leqslant a$ $E_3(z) = E_1;\ a \leqslant z \leqslant 0.5h,\ 0 \leqslant \frac{a}{h} \leqslant 0.5$
	Imperfect FGMs (Case-II): $E_1(z) = E_2 + (E_1 - E_2)\left(\frac{1}{2} + \frac{z}{h}\right)^k;\ 0 \leqslant z \leqslant 0.5h$ $E_2(z) = E_2 + (E_1 - E_2)\left(\frac{1}{2} + \frac{z}{h}\right)^k;\ -b \leqslant z \leqslant 0$ $E_3(z) = E_2;\ -0.5h \leqslant z \leqslant -b,\ -0.5 \leqslant \frac{b}{h} \leqslant 0$

$$A_{33}\frac{d^3u}{dx^3} - D_{12}\frac{d^4w_b}{dx^4} - D_{22}\frac{d^4w_s}{dx^4} + N^0_{xx}\frac{d^2w_b}{dx^2} + \left(A_{44} + N^0_{xx}\right)\frac{d^2w_s}{dx^2} + (A_{44} + D_{55})\frac{d^2w_z}{dx^2} = 0 \tag{14c}$$

$$-A_{66}\frac{du}{dx} + A_{77}\frac{d^2w_b}{dx^2} + A_{44}\frac{d^2w_z}{dx^2} + (A_{44} + A_{88})\frac{d^2w_s}{dx^2} - A_{55}w_z = 0 \tag{14d}$$

3. Solving approach

To procure the numerical outputs of critical stability of the FGM beam with the deemed imperfection, here the Galerkin technique is used referring to the first mode of buckling. This method is a kind of weighted residual methods (WRMs). To exploit it, we presume a residue for the equations where the residue is errors of equations. Indeed, the approximation causes the errors. If we utilize an exact solution, so the residuals become zero. WRMs are on the basis of attaining an approximation solution for which the average of residue over the domain is assumed to be zero. It can be obtained by a weight function (X_m) so that the weighted integral equals to zero. This weight function satisfies a variety of boundary conditions (BCs). Generally, the weighting function should be multiplied with the residue and then integration across the whole domain [0, L] is accomplished. In this regard, the following functions can be executed.

- Pinned-Pinned BCs (S-S):

$$X_m(x) = \sin(\alpha_m x) \tag{15a}$$

- Clamped-Clamped BCs (C–C):

$$X_m(x) = \frac{1}{2}[1 - \cos(2\alpha_m x)] \tag{15b}$$

- Clamped-Pinned BCs (C–S):

$$X_m(x) = 0.170938\left[\sin(\beta_m x) - \beta_m L\cos(\beta_m x) + \beta_m L\left(1 - \frac{x}{L}\right)\right] \tag{15c}$$

- Clamped-Free BCs (C–F):

$$X_m(x) = \sin(\gamma_m x) \times \cos(\gamma_m x) \tag{15d}$$

in which $\alpha_m = \frac{m\pi}{L}$, $\beta_m = 1.4318\frac{m\pi}{L}$, $\gamma_m = \frac{m\pi}{4L}$.

As such, the assumed displacements can be taken as below [11]

$$u(x) = \sum_{m=1}^{\infty} U_m \frac{\partial X_m(x)}{\partial x} \tag{16a}$$

$$w_b(x) = \sum_{m=1}^{\infty} W_{bm} X_m(x) \tag{16b}$$

$$w_s(x) = \sum_{m=1}^{\infty} W_{sm} X_m(x) \tag{16c}$$

$$w_z(x) = \sum_{m=1}^{\infty} W_{zm} X_m(x) \tag{16d}$$

In the present study, we are using Sine or Cosine functions as weight functions and the Sine and Cosine are continuously differentiable in the whole domain. So, this will behave like an analytical method, and the rate of convergence will be irrelevant. That is why the convergence rate is not assessed and m denotes mode numbers.

Then, with imposing Eq. (16) in Eq. (14), the matrix form of constitutive equation of the problem can be regulated as

$$\begin{bmatrix} K_{11} & K_{12} & K_{13} & K_{14} \\ K_{21} & K_{22} & K_{23} & K_{24} \\ K_{31} & K_{32} & K_{33} & K_{34} \\ K_{41} & K_{42} & K_{43} & K_{44} \end{bmatrix} \begin{Bmatrix} U_m \\ W_{bm} \\ W_{sm} \\ W_{zm} \end{Bmatrix} = 0 \tag{17}$$

in which $\left[K_{ij}\right]_{4\times4}$ is the matrix coefficients for the FGM beam. If the determinant of the matrix equals to zero, one can acquire the non-trivial solution as

$$\det\left[K_{ij}\right]_{4\times4} = 0 \tag{18}$$

The output of this operation would be an algebraic polynomial equation based on the one unknown (N^0_{xx}), which solving this equation generates the critical buckling loads.

The components of the coefficients matrix are exploded in Appendix A.

4. Credibility of results

This part of the present research is assigned to demonstrate the validity and punctuality of the closed-form solution, in particular the new shape function of shear deformation distribution. First off, most of the momentous theories of shear deformation variations are listed in Table 2, next to each other.

To estimate the aforementioned shape functions, Figs. 4a and 4b are designed in which some shape functions are drawn. As seen, the proposed shape function is in very good parallelism with other functions. More comparisons can be observed by Tables 3 and 4 for which also results of the finite element method (FEM) are added. It is worth noticing that the results of FEM are given based on the 1D beam element and using a suitable number of elements and nodes depending on the cross-section and length of the beam. As can be found, the results of the proposed shape function can be permitted to use as correlation of results is simply seen.

After reaching a concordance for the new shape function proposed in this research and understanding its very good balancing against

Table 2
Shape functions for shear stress distribution in literature.

Reference	*f(z)*	*Mathematical view*
Zenkour [72]	$h\sinh\frac{z}{h} - \frac{4}{3}\frac{z^3}{h^2}\cosh\left(\frac{1}{2}\right)$	HT
Touratier [73]	$\frac{h}{\pi}\sin\left(\frac{\pi}{h}z\right)$	T
Shahsavari et al. [11]	$-\left[r_1\left(\frac{z}{h}\right) + r_2\sinh\left(\frac{z}{h}\right)\right]h^*$	HT
Zohra Zaoui et al. [12]	$\frac{\pi h}{\pi^4+h^4}\left[\left(\pi^2\sin\left(\frac{\pi z}{h}\right) + h^2\cos\left(\frac{\pi z}{h}\right)\right)\exp\left(\frac{hz}{\pi}\right) - h^2\right]$	T/Ex-2
Akavci and Tanrikulu [8]	$3.7z\left(1.27sech^{0.65}\left(\frac{z}{h}\right) - 1\right)$	HT
Reddy [7]	$z\left(1 - \frac{4}{3}\frac{z^2}{h^2}\right)$	Pol
Mantari et al. [74]	$\tan(rz) - zr\sec^2\left(\frac{rh}{2}\right)$; $[r = 0.2]$	T
Joshan et al. [75]	$\frac{r}{\pi}csch^{-1}\left(\frac{rh}{z}\right) - z\frac{2r}{h^2\sqrt{(4r^2+1)}}$; $[r = 0.32]$	HT
Neves et al. [76]	$\sin\left(\frac{\pi}{h}z\right)$	T
Neves et al. [77]	$\sinh\left(\frac{\pi}{h}z\right)$	HT
Sarangan and Singh [78]	$\tanh\left(\frac{rz}{h}\right) - z\frac{r}{h}sech^2\left(\frac{r}{2}\right)$; $[r = 2.5]$	HT
Aydogdu [79]	$\left(1 - 4\frac{z^2}{h^2}\right)r^{\left(\frac{2z^2}{h^2\ln(r)}\right)}$; $[r = 3]$	Ex-1/Log
Soldatos [80]	$h\sinh\left(\frac{z}{h}\right) - z\cosh\left(\frac{1}{2}\right)$	HT
Karama et al. [81]	$z\exp\left(-2\left(\frac{z}{h}\right)^2\right)$	Ex-2
Thai and Choi [82]	$-\frac{z}{4} + \frac{5z^3}{3h^2}$	Pol
Hebali et al. [83]	$\frac{\frac{h}{2}\sinh\left(\frac{2z}{h}\right) - z}{\cosh\left(\frac{z}{h}\right) - 1}$	HT
Present	$\tanh\left(\frac{z}{h} - \frac{z^3}{h^3} - r\frac{z^5}{h^5}\right)$; $[r = 0.8]$	HT/Pol

HT = Hyperbolic Trigonometric.
Ex-1 = Exponential function form A.
Ex-2 = Exponential function form B.
Pol = Polynomial.
Log = Logarithmic.
T = Trigonometric.
* $r_1 = \frac{\cosh(\theta)}{24\sinh(\theta) - 11\cosh(\theta)} - 1$, $r_2 = \frac{-1}{24\sinh(\theta) - 11\cosh(\theta)}$, $\theta = \frac{1}{2}$.

Table 3
Elastic buckling loads (*kN*) for several shape functions in a S-S square steel column based on HSDT ($E = 2 \times 10^5 MPa$, $h = 60\ mm$).

Function	*L/h*			
	10	15	20	30
Zenkour [72]	5813.68	2610.32	1473.59	656.617
Touratier [73]	5813.25	2610.24	1473.56	656.612
Shahsavari et al. [11]	5807.16	2609.01	1473.17	656.534
Zohra Zaoui et al. [12]	5921.76	2631.89	1480.44	657.974
Akavci and Tanrikulu [8]	5813.36	2610.26	1473.57	656.613
Reddy [7]	5813.68	2610.33	1473.59	656.617
Mantari et al. [74]	5921.76	2631.89	1480.44	657.974
Joshan et al. [75]	5825.87	2612.78	1474.37	656.772
Neves et al. [76]	5824.64	2612.53	1474.29	656.757
Neves et al. [77]	5827.76	2613.16	1474.49	656.796
Sarangan and Singh [78]	5825.14	2612.63	1474.33	656.763
Aydogdu [79]	5826.05	2612.82	1474.39	656.775
Soldatos [80]	5829.55	2613.52	1474.61	656.819
Karama et al. [81]	5812.89	2610.17	1473.54	656.607
Thai and Choi [82]	5847.56	2617.13	1475.76	657.047
Hebali et al. [83]	5847.35	2617.09	1475.75	657.045
Present	5825.92	2612.79	1474.37	656.773

literature, the further acknowledgments of numerical outcomes are tabulated by Tables 5–12. This deliberation dedicates outputs of the Euler-Bernoulli (EB) beam model, a modified first-order shear deformation theory (S-FSDT), higher-order shear deformation theory without thickness stretching effect (HSDT, $\varepsilon_z = 0$), and with considering this effect ($\varepsilon_z \neq 0$), and FEM [84]. Note that both HSDT and the new theory are based on using the present shape function. In doing so, the beam is debated in two cross-sectional shapes, namely square and rectangular. Moreover, the S-S, F-F, and C–C edge conditions are discussed. For Tables 5–8, the behavioral of the beam is based on a thin material as $45 < L/h < 60$ for the square and $65 < L/h < 90$ for the rectangular one, but Tables 9-12 are prepared for a thick and very thick material as $2.5 < L/h < 12.5$ for the square beam and $3.5 < L/h < 18.5$ for the rectangular beam. For Tables 5 and 6, one can see that the results of EB and S-FSDT are not in an excellent agreement with those of HSDT, HPET as well as FEM. Albeit while the beam is enlarging, the results of all the theories are in the neighborhood. Furthermore, considering Tables 7 and 8 presents equivalent results for all theories, although some discrepancies can be found. By this part of the comparison, one can conclude that the importance of shear deformations is more and more obvious by having less flexible edge conditions.

On the other hand, thick and very thick beams are concerned with the rest of the Tables (Tables 9–12). Within these Tables, the significance of shear deformations is noticeably found. As can also be seen, the results of HPET are more accurate than HSDT. More importantly, it can be stated that when a beam is in the zone of a very thick beam, even HSDT results fail and a higher-order beam theory based on the stretching effect should be taken in use. As far as we investigate a non-flexible boundary condition i.e. C–C, the huge conflicts between all theories are clearer. To conclude, it is worth mentioning to say that the difference between HSDT and HPET can be further ascertained by C–C.

5. Stability of an imperfect FGM beam

To determine and report the structural response of the defected FGM in a stability problem, the material specifications are collected in Table 13. It is germane to note that in this section we are going to examine two types of FGM beams, the first case (I) is the customary

Table 4
Elastic buckling loads (*kN*) for several shape functions in a F-F square steel column based on HSDT ($E = 2 \times 10^5 MPa$, $h = 60\ mm$).

Method	*L/h*			
	10	15	20	30
FEM (ABAQUS)	1471	656.10	369.52	164.38
Function				
Zenkour [72]	1473.59	656.61	369.68	164.40
Touratier [73]	1473.56	656.61	369.68	164.40
Shahsavari et al. [11]	1473.17	656.53	369.65	164.40
Zohra Zaoui et al. [12]	1480.44	657.97	370.11	164.49
Akavci and Tanrikulu [8]	1473.57	656.61	369.68	164.40
Reddy [7]	1473.59	656.61	369.68	164.40
Mantari et al. [74]	1480.44	657.97	370.11	164.49
Joshan et al. [75]	1474.37	656.77	369.73	164.41
Neves et al. [76]	1474.29	656.75	369.72	164.41
Neves et al. [77]	1474.49	656.79	369.73	164.42
Sarangan and Singh [78]	1474.33	656.76	369.72	164.42
Aydogdu [79]	1474.39	656.77	369.73	164.42
Soldatos [80]	1474.61	656.82	369.74	164.42
Karama et al. [81]	1473.54	656.60	369.67	164.41
Thai and Choi [82]	1475.76	657.05	369.82	164.43
Hebali et al. [83]	1475.75	657.04	369.82	164.43
Present	1474.37	656.77	369.73	164.42

Table 5
Elastic buckling load (kN) for a S-S square steel column ($E = 2 \times 10^5 MPa$, $h = 60\ mm$).

$L\ (m)$	EB	$S\text{-}FSDT$, $k_s = 5/6$	$Present$		FEM [84]
			$\varepsilon_z = 0$	$\varepsilon_z \neq 0$	
2.75	281.895	281.891	281.675	281.631	281.550
3	236.871	236.867	236.715	236.684	236.630
3.25	201.830	201.828	201.717	201.695	201.650
3.5	174.027	174.026	173.944	173.927	173.900

Table 6
Elastic buckling load (kN) for a S-S rectangular steel column ($E = 2 \times 10^5 MPa$, $h = 40\ mm$, $b = 90\ mm$).

$L\ (m)$	EB	$S\text{-}FSDT$, $k_s = 5/6$	$Present$		FEM [84]
			$\varepsilon_z = 0$	$\varepsilon_z \neq 0$	
2.75	125.287	125.284	125.244	125.235	125.122
3	105.276	105.274	105.245	105.239	105.230
3.25	89.702	89.700	89.680	89.676	89.668
3.5	77.345	77.344	77.329	77.326	77.320

Table 7
Elastic buckling load (kN) for a F-F square steel column ($E = 2 \times 10^5 MPa$, $h = 60\ mm$).

$L\ (m)$	EB	$S\text{-}FSDT$, $k_s = 5/6$	$Present$		FEM [84]
			$\varepsilon_z = 0$	$\varepsilon_z \neq 0$	
2.75	70.474	70.473	70.460	70.457	70.452
3	59.218	59.217	59.207	59.206	59.202
3.25	50.458	50.457	50.450	50.449	50.447
3.5	43.507	43.506	43.503	43.500	43.499

Table 8
Elastic buckling load (kN) for a F-F rectangular steel column ($E = 2 \times 10^5 MPa$, $h = 40\ mm$, $b = 90\ mm$).

$L\ (m)$	EB	$S\text{-}FSDT$, $k_s = 5/6$	$Present$		FEM [84]
			$\varepsilon_z = 0$	$\varepsilon_z \neq 0$	
2.75	31.322	31.321	31.319	31.318	31.318
3	26.319	26.318	26.317	26.316	26.316
3.25	22.426	22.425	22.424	22.423	22.423
3.5	19.336	19.336	19.335	19.335	19.335

Table 9
Elastic buckling load (kN) for a very thick and thick S-S square steel column ($E = 2 \times 10^5 MPa$, $h = 60\ mm$).

$L\ (m)$	EB	$S\text{-}FSDT$, $k_s = 5/6$	$Present$	
			$\varepsilon_z = 0$	$\varepsilon_z \neq 0$
0.15	94748.2	94252.1	74996.4	72063.1
0.25	34109.4	34044.8	31155.4	30634.1
0.5	8527.34	8523.3	8329.89	8292.05
0.75	3789.93	3789.13	3750.42	3742.72
1	2131.83	2131.58	2119.28	2116.82
1.25	1364.37	1364.27	1359.22	1358.21

case, namely composition of ceramic and metal, and then the second case (II) is a compound of alumina and aluminium. Subsequently, under various sorts of boundary conditions, parametric studies on the thick and very thick FGM beams are plotted.

To gain the critical buckling loads, we introduce a dimensionless relation as

$$P_{Cr} = 100 \times \frac{N^0_{xx}}{E_2 h^2} \tag{19}$$

Table 10
Elastic buckling load (kN) for a very thick and thick F-F square steel column ($E = 2 \times 10^5 MPa$, $h = 60\ mm$).

$L\ (m)$	EB	$S\text{-}FSDT$, $k_s = 5/6$	$Present$	
			$\varepsilon_z = 0$	$\varepsilon_z \neq 0$
0.15	23687.1	23655.9	22223.8	21956.9
0.25	8527.34	8523.3	8329.89	8292.05
0.5	2131.83	2131.58	2119.28	2116.82
0.75	947.482	947.432	944.993	944.504

Table 11
Elastic buckling load (kN) for a very thick and thick C–C square steel column ($E = 2 \times 10^5 MPa$, $h = 60\ mm$).

$L\ (m)$	EB	$S\text{-}FSDT$, $k_s = 5/6$	$Present$	
			$\varepsilon_z = 0$	$\varepsilon_z \neq 0$
0.15	378993.1	371178.1	184561.1	168539.1
0.25	136437.1	135411.1	98921.2	93937.6
0.5	34109.4	34044.8	31155.4	30634.9
0.75	15159.7	15147.1	14546.7	14431.9

Table 12
Elastic buckling load (kN) for a very thick and thick F-F rectangular steel column ($E = 2 \times 10^5 MPa$, $h = 40\ mm$, $b = 90\ mm$).

$L\ (m)$	EB	$S\text{-}FSDT$, $k_s = 5/6$	$Present$	
			$\varepsilon_z = 0$	$\varepsilon_z \neq 0$
0.15	10527.6	10506.8	10228.43	10171.3
0.25	3789.93	3787.24	3750.45	3742.72
0.5	947.482	947.314	944.995	944.50
0.75	421.103	421.07	420.61	420.51

Table 13
Marerial parameters.

FGM beam-I [85–88]	Ceramic: Silicon Carbide (Si_3C_4) $E_1 = 348GPa$, $\nu_1 = 0.24$ Metal:Stainless Steel-Grade 304 (AISI 304) $E_2 = 200GPa$, $\nu_2 = 0.29$
FGM beam-II [8]	Alumina: (Al_2O_3) $E_1 = 380GPa$, $\nu_1 = 0.3$ Aluminium: (Al) $E_2 = 70GPa$, $\nu_2 = 0.3$

In Figs. 5a–d, we examine the role of the incomplete FGM beams in a thick manner and in the two states and patterns mentioned before for two types of FGM beams. In Fig. 5a, the variation of the volume fraction parameter is seen in both perfect and imperfect matter states. The incomplete matter of this figure follows the pattern of the first case. That is, in the case of the FGM composite material, the amount of pure ceramic area is substantial in the thickness of the beam. For this purpose, $a = 0.2$ h was chosen. Also, $a = 0.5$ h is the perfect state of FGM. As can be seen, when $k = 0$ (the whole beam is full of ceramic), the value of parameter a does not make any difference in the results. That is quite logical. But as the parameter k increases and the metal composition is added, it can be seen that as we move toward the beam with pure metal ($k = \infty$), the results will be disparate. However, the incomplete FGM beam, in this case, is much more resistant than the perfect case because of the increased ceramic powder content in the composite material. This result is due to the higher modulus of elasticity for ceramic. Interestingly, the difference in results with the more rigid boundary conditions increases. This means that the less flexible the boundary condition and, indeed, the lower the degrees of freedom of the two ends of the beam, the greater the impact of the defect. In terms of diagrams, the maximum effect is on the boundary condition of the clamped and the least on the free edges.

On the other hand, Fig. 5c is designed for the second defect pattern, in which the pattern of the metallic area will be remarkable in the thickness and will not be confined to the lowest layer. Here, $b = 0.5$ h means perfect beam, and $b = 0.2$ h means imperfect beam, which accounts for about 30% of the thickness with the pure metal area with the remainder being a combination of two metal and ceramic materials (Fig. 3b). By examining this figure, we can see that when the numerical value of the power-law index is $k \leq 1$, due to the presence of ceramic in the composite material, it is important to determine how much metal has formed in the thickness. However, by increasing the parameter k as we approach the rich-metal beam and the ceramic content is negligible, the defect importance in this model is also eliminated, and the results in both perfect and defected beams are matched. The important point here is for the results $k < 1$, which the difference between the results confirms this. In fact, this incomplete case may be more important in the stability analysis than the previous case. Because FGM beams are used in product design assuming a complete pattern, which in regard to a complete FGM beam the safety factor is assured for them. According to the above figure, it can be stated that if the metal region is not unique to the lowest layer of thickness, and some part of the thickness forms with pure metal, the stability of the composite material will be far less than that of the perfect material, resulting in unpredictable failure and yield with loads lower than the loads designed for the criterion. This underlines the

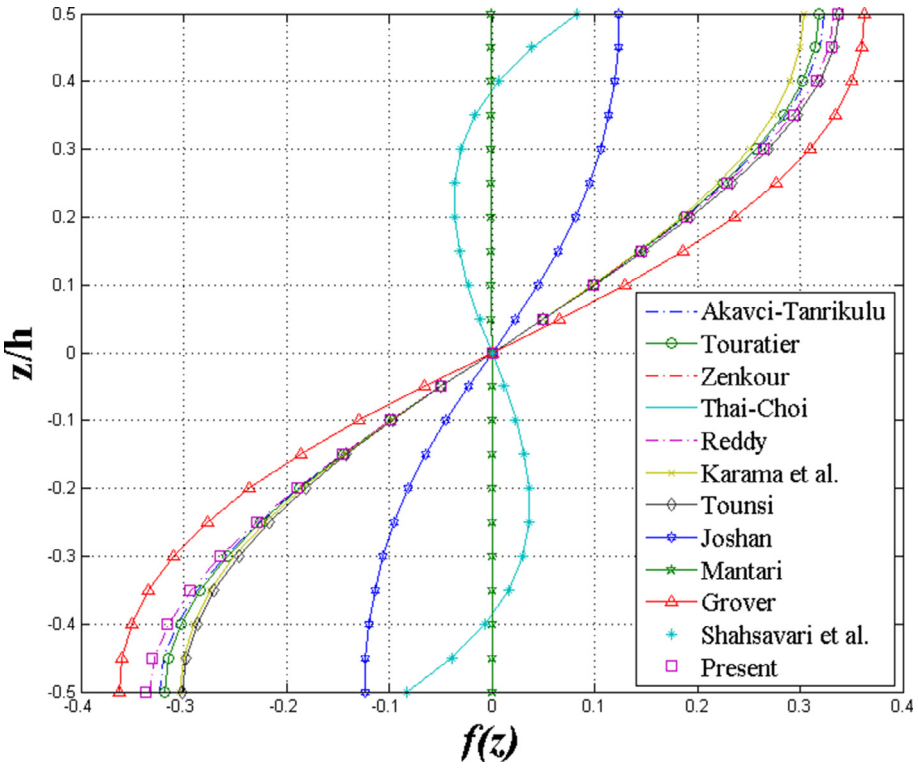

Fig. 4a. Shear deformation functions based on the literature.

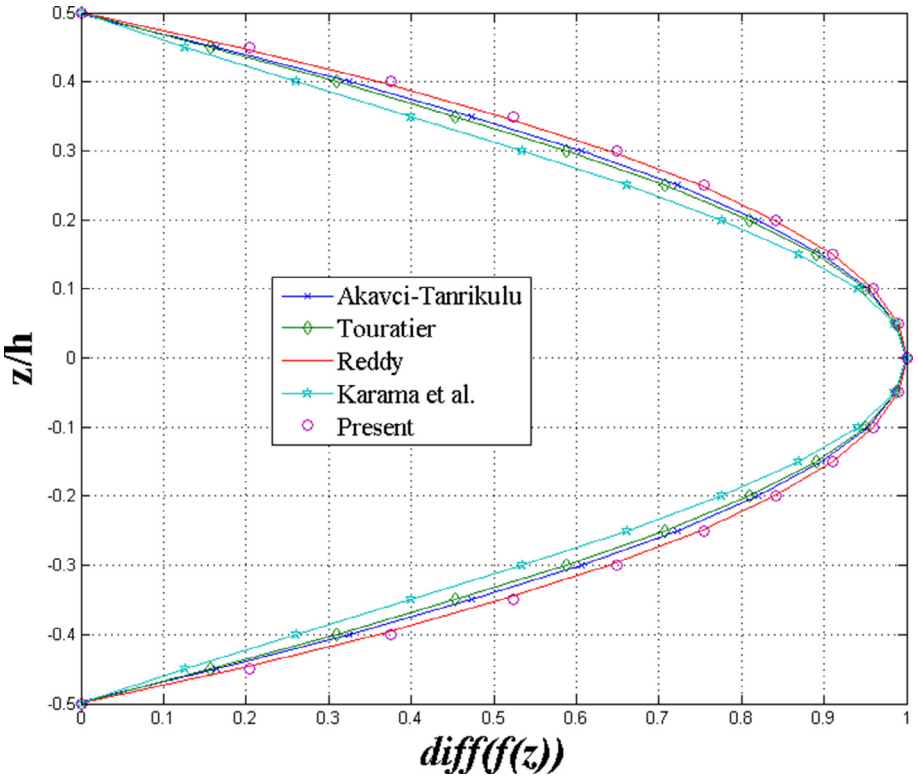

Fig. 4b. Variation of shear deformation functions based on the literature.

significance of examining defective cases for products made of FGM materials.

Under other conditions, regarding Figs. 5b and 5d, we are trying to investigate the FGM beam-II as well as compare its results with the first type of beam. Fig. 5b is drawn exactly as same as Fig. 5a but the alumina and aluminium are respectively replaced with the ceramic and metal. It is in a clear view that the results here are further remarkable than those of the two other figures, that is, the imperfection

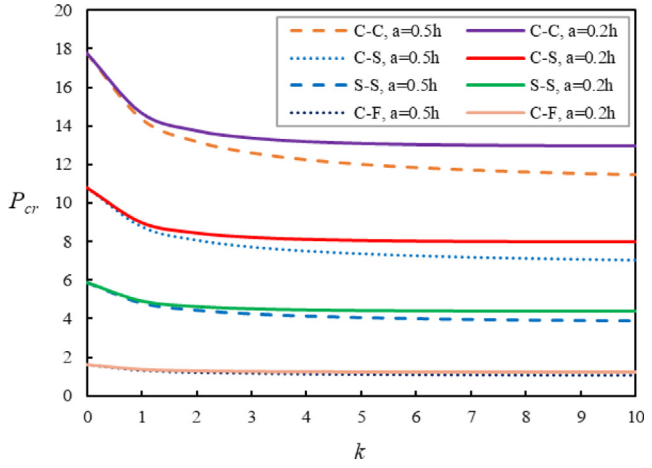

Fig. 5a. Power-law index vs. different edge conditions for a thick FGM beam-I (Case *I*, $L = 5\ h$).

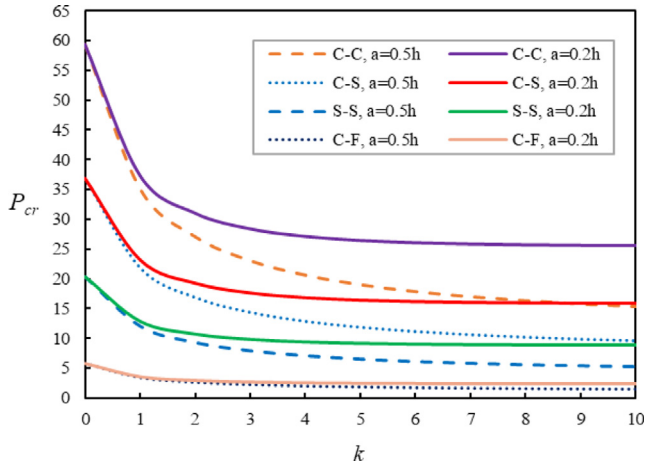

Fig. 5b. Power-law index vs. different edge conditions for a thick FGM beam-II (Case *I*, $L = 5\ h$).

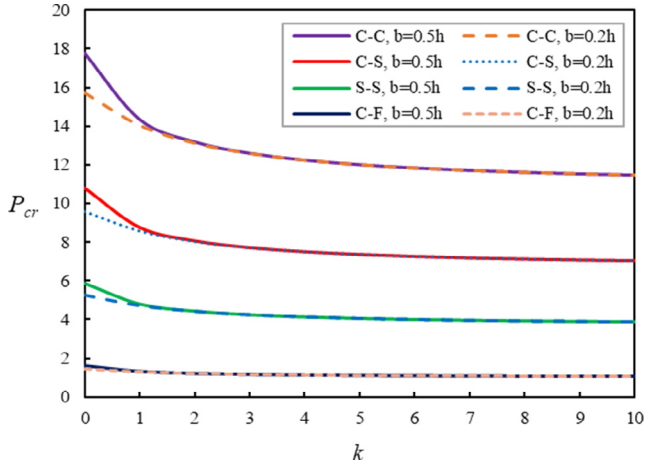

Fig. 5c. Power-law index vs. different edge conditions for a thick FGM beam-I (Case *II*, $L = 5\ h$).

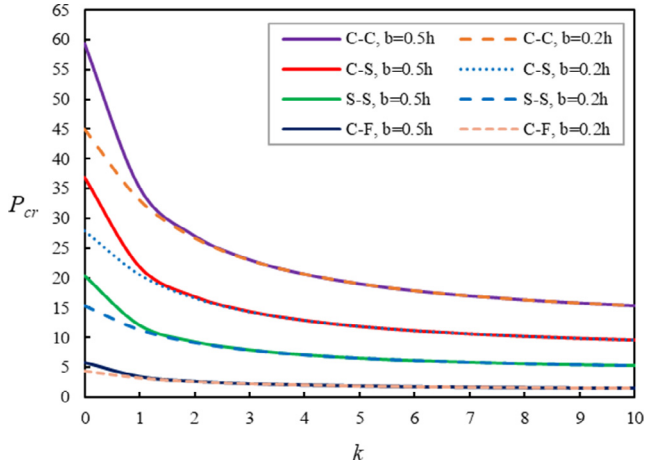

Fig. 5d. Power-law index vs. different edge conditions for a thick FGM beam-II (Case *II*, $L = 5\ h$).

impact is more visible. In point of fact, the difference between values of two mixed materials can directly affect this finding. In addition to these, for Figs. 5b and 5d, an intensive fall can be observed for results between $k = 0$ and $k = 1$. This can be in light of the difference in the elasticity modulus of two mixed materials. This means, going from pure alumina state into the FGM compound leads to such the behavior.

With the help of Figs. 6a-d and in conformity with Figs. 5a-d, but here we will continue to look for a very thick beam ($L = 2\ h$). First, we should state that the difference in results between the two perfect and incomplete cases can be seen more seriously in diagrams of Figs. 6, which can lead to the conclusion that the thicker the beam, the greater the defect effect. Another important point to note may be that the difference in the results of the C–C, S–S and C–S boundary conditions is increased against the free boundary condition and subsequently the difference of their results decreases with each other as the beam thickens. The comparison between Figs. 5 and 6 illustrates vividly this result.

Figs. 7a–d are presented for a more complete examination of the defects in both patterns. In Fig. 7a, which represents the first defect pattern, the diagram starts from the case where $a = 0$, which means that half the thickness is made up of the pure ceramic area. The end

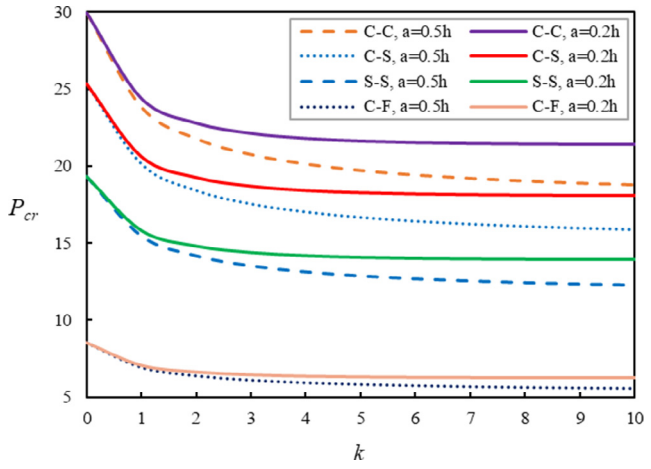

Fig. 6a. Power-law index vs. different edge conditions for a very thick FGM beam-I (Case *I*, $L = 2\ h$).

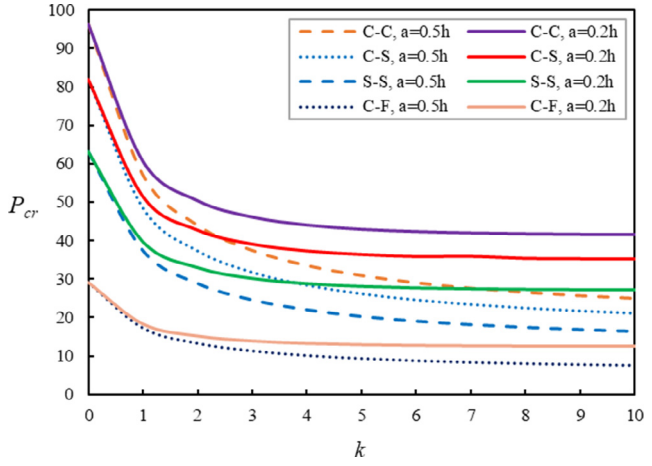

Fig. 6b. Power-law index vs. different edge conditions for a very thick FGM beam-II (Case *I*, $L = 2\,h$).

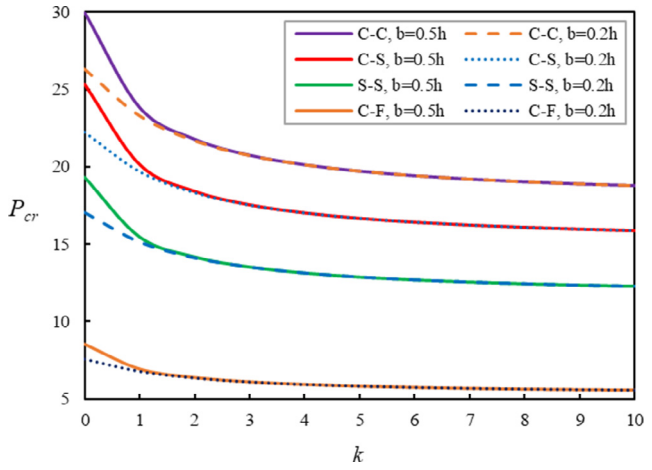

Fig. 6c. Power-law index vs. different edge conditions for a very thick FGM beam-I (Case II, L = 2 h).

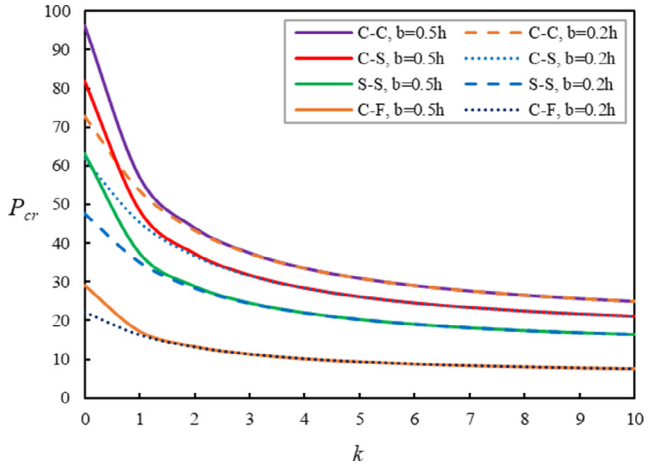

Fig. 6d. Power-law index vs. different edge conditions for a very thick FGM beam-II (Case *II*, $L = 2\,h$).

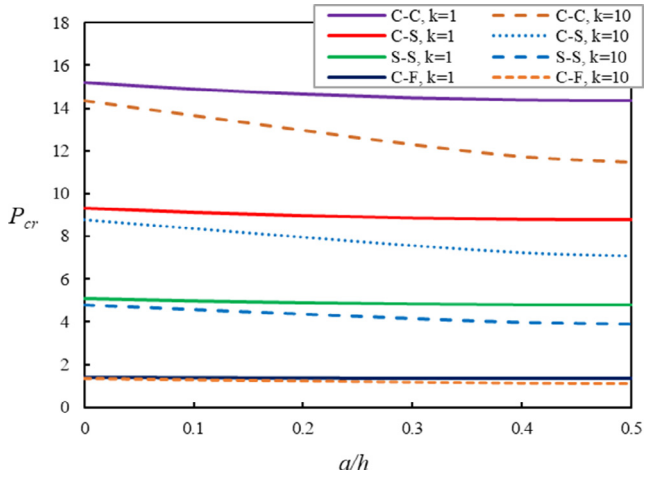

Fig. 7a. The first pattern of imperfection vs. different edge conditions for a thick FGM beam-I ($L = 5\,h$).

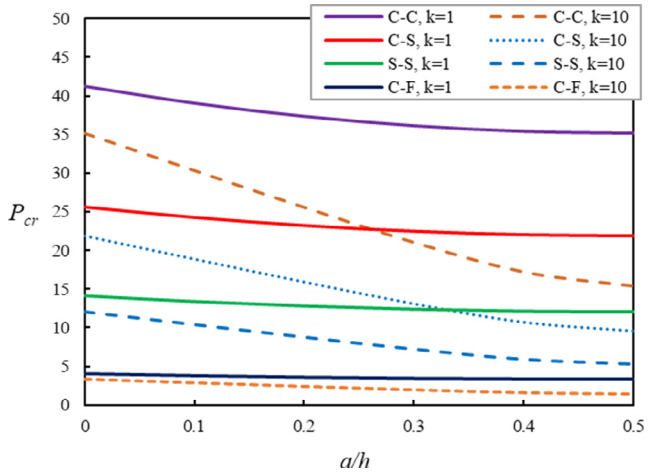

Fig. 7b. The first pattern of imperfection vs. different edge conditions for a thick FGM beam-II ($L = 5\,h$).

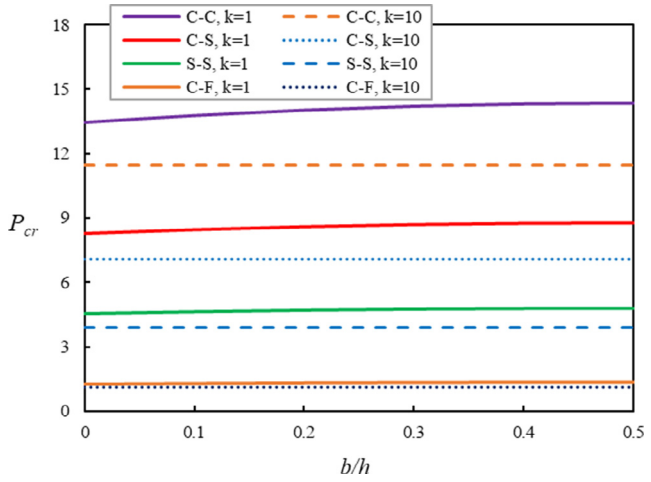

Fig. 7c. The second pattern of imperfection vs. different edge conditions for a thick FGM beam-I ($L = 5\,h$).

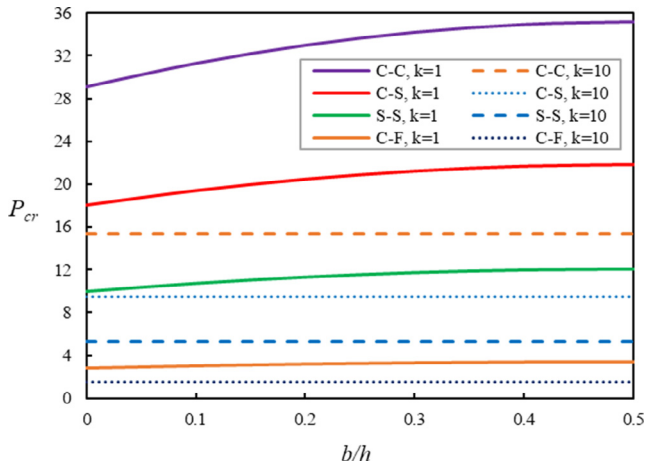

Fig. 7d. The second pattern of imperfection vs. different edge conditions for a thick FGM beam-II ($L = 5\ h$).

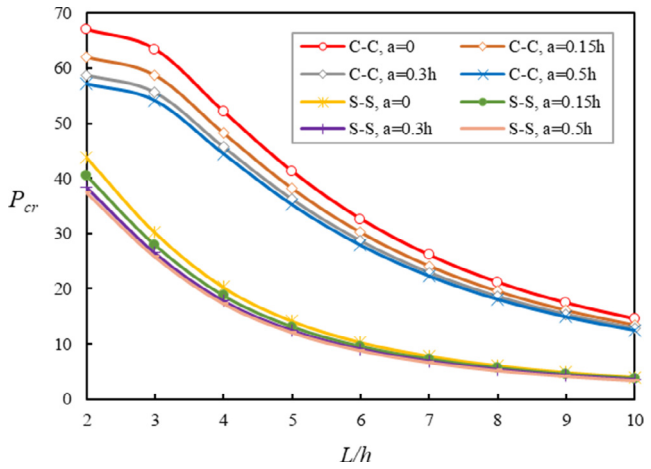

Fig. 8b. Slenderness ratio vs. different edge conditions for an FGM beam-II (Case *I*, $k = 1$).

of the horizontal axis is $a = 0.5$ h, which shows the perfect state. The same is true in Fig. 7c, that is, when $b = 0$, we can say that half the thickness is formed by pure metal, and $b = 0.5$ means a perfect FG beam. Both modes are provided for a thick beam. As can be seen, with increasing a/h and b/h values, the stability of the composite beam decreases and increases, respectively. It should be remembered that the increase of a means decreasing the amount of ceramic in the composite material, while the increase of b means of decreasing the amount of metal powder in the mixed material. As it turns out, the defect in the FGM material does not affect strikingly the free edge boundary condition. The physical reason for this may be that the stability of an FGM beam is at maximum affected by defect when the beam itself can exhibit maximum resistance. In point of fact, this will be possible when the degrees of freedom of both ends of the beam are reduced.

Elseway, regarding Figs. 7b and 7d, the FGM beam-II is assessed precisely similar to Figs. 7a and 7c. Fig. 7b shows quite equivalent with Fig. 7a but the alumina and aluminium are respectively substituted with the ceramic and metal. The prominence of the imperfection effect is here easily seen compared with the two other figures. This influence is evidently more prominent for C–C end conditions than others.

Finally, by presenting Figs. 8a–d, we desire to investigate the effect of the dimensionless parameter of slenderness ratio (L/h) on both

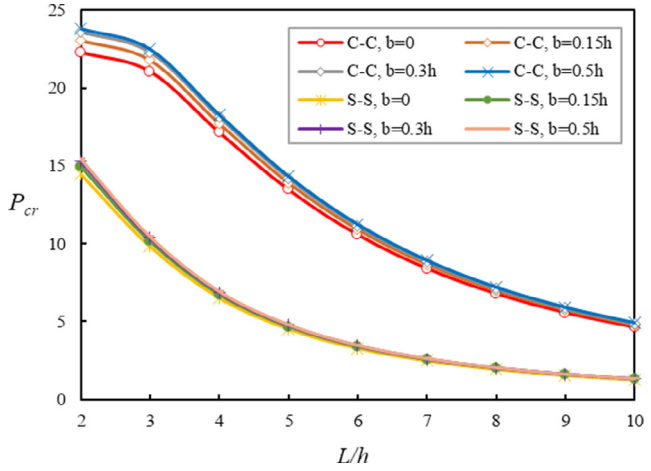

Fig. 8c. Slenderness ratio vs. different edge conditions for an FGM beam-I (Case *II*, $k = 1$).

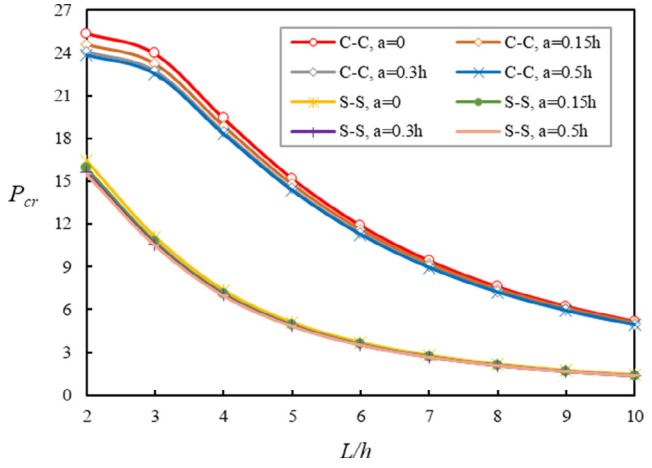

Fig. 8a. Slenderness ratio vs. different edge conditions for an FGM beam-I (Case *I*, $k = 1$).

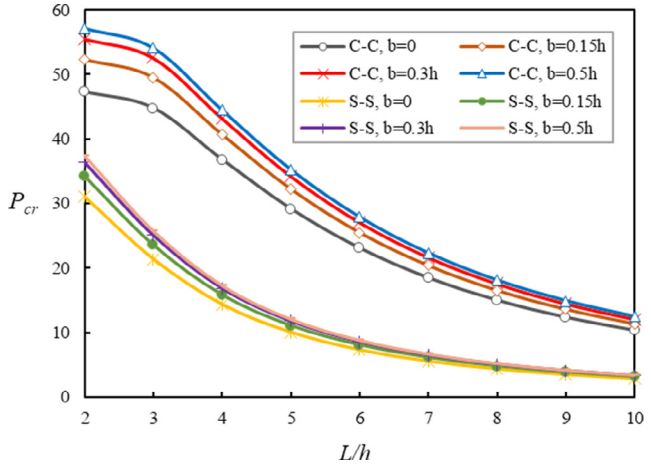

Fig. 8d. Slenderness ratio vs. different edge conditions for an FGM beam-II (Case *II*, $k = 1$).

defect patterns. The first pattern is displayed in Figs. 8a and 8b and the second pattern is devoted in Figs. 8c and 8d for the two kinds of beams, respectively. The figures are a linearly distribution of metal and ceramic or alumina and aluminium. The results are obtained for the two C–C and S–S boundary conditions. The interesting point in these figures can be that by increasing the length-to-thickness ratio, the slope of results of the C–C boundary condition has no regularity like the hinge boundary condition. The reduction slope of the result at the S-S boundary condition is smooth and gradual. However, this decreasing trend in the C–C will be at initial with a low slope and then with a steeper gradient after $L/h = 3$. The reason may be that if the beam is thicker or thinner, it has gradual importance on boundary conditions, and the behavior is diverse for various end conditions. Hence, it is important that the beam be thin, thick, or very thick, and results will go with the fall for end conditions with lower degrees of freedom. For this reason, the behavior of the curve results in a break. On the other hand, it is quite obvious that in very large L/h values the significance of boundary conditions and consequently the defect will be negligibly small.

6. Conclusions

A defect in the material composition of FGM beams was investigated in this paper. Moreover, the influence of stretching in thickness layers was examined by a higher-order elasticity theory (HPET). An analytical solution was achieved to give the axial buckling behavior of thick FGM beams on the basis of variants of end conditions. Plus, a novel shear deformation shape function was proposed based on the hyperbolic-polynomial functions. To obtain the mathematical model of the problem, energy principle and linear Lagrangian strain have assisted. A full validation was prepared to assure the quality of the new shape function. The imperfect FGM was analyzed with tabular and pictorial numerical outcomes. The study generated some new findings summarized below,

* The flexibility of boundary conditions directly affects the significance of shear deformations.
* The EB and S-FSDT can be applicable for thin ($20 < L/h < \infty$) and moderately thick beams ($10 < L/h < 20$), respectively. And for thick beams ($5 < L/h < 10$) their results fail and the higher-order elasticity theories based on modified shear deformations should be used. However, when the material falls within the range of a very thick beam ($1 < L/h < 5$) the results of the common higher-order theories fail, and the higher-order theories based on including the stretching effect should be taken into consideration while there is difficulty to use of exact-3D.
* The less-flexible the boundary conditions, the more impact the imperfections.
* The thicker the beam, the more prominent the influence of imperfections.
* A drawback to the material composition of FGMs can lead to disparate responses of such composite materials against mechanical loading. This behavior which is dependent entirely on the difference between the two materials' elasticity features can give an unpredictable reaction if the basic concept and safety factor of designing of parts and products made of FGMs are based on the perfect power-law mixture.

CRediT authorship contribution statement

Mohammad Malikan: Conceptualization, Methodology, Investigation, Software, Validation, Writing - original draft. **Victor A. Eremeyev:** Methodology, Writing - review & editing, Supervision, Funding acquisition.

Declaration of Competing Interest

The authors declare that they have no known competing financial interests or personal relationships that could have appeared to influence the work reported in this paper.

Acknowledgement

V.A.E. was supported by the grant of the Government of the Russian Federation (contract No. 14.Y26.31.0031).

Appendix A

$$K_{11} = A_{11}\int_0^L \left(\frac{d^3X_m}{dx^3}\frac{dX_m}{dx}\right)dx$$

$$K_{12} = -A_{12}\int_0^L \left(\frac{d^3X_m}{dx^3}X_m\right)dx$$

$$K_{13} = -A_{33}\int_0^L \left(\frac{d^3X_m}{dx^3}X_m\right)dx$$

$$K_{14} = D_{33}\int_0^L \left(\frac{dX_m}{dx}X_m\right)dx$$

$$K_{21} = A_{12}\int_0^L \left(\frac{d^4X_m}{dx^4}\frac{dX_m}{dx}\right)dx$$

$$K_{22} = \int_0^L \left(-D_{11}\frac{d^4X_m}{dx^4}X_m + N^0_{xx}\frac{d^2X_m}{dx^2}X_m\right)dx$$

$$K_{23} = \int_0^L \left(-D_{12}\frac{d^4X_m}{dx^4}X_m + N^0_{xx}\frac{d^2X_m}{dx^2}X_m\right)dx$$

$$K_{24} = D_{44}\int_0^L \left(\frac{d^2X_m}{dx^2}X_m\right)dx$$

$$K_{31} = A_{33}\int_0^L \left(\frac{d^4X_m}{dx^4}\frac{dX_m}{dx}\right)dx$$

$$K_{32} = \int_0^L \left(-D_{12}\frac{d^4X_m}{dx^4}X_m + N^0_{xx}\frac{d^2X_m}{dx^2}X_m\right)dx$$

$$K_{33} = \int_0^L \left[-D_{22}\frac{d^4X_m}{dx^4}X_m + (A_{44} + N^0_{xx})\frac{d^2X_m}{dx^2}X_m\right]dx$$

$$K_{34} = \int_0^L \left[(A_{44} + D_{55})\frac{d^2X_m}{dx^2}X_m\right]dx$$

$$K_{41} = -A_{66}\int_0^L \left(\frac{d^2X_m}{dx^2}\frac{dX_m}{dx}\right)dx$$

$$K_{42} = A_{77}\int_0^L \left(\frac{d^2X_m}{dx^2}X_m\right)dx$$

$$K_{43} = \int_0^L \left[(A_{44}+A_{88})\frac{d^2X_m}{dx^2}X_m\right]dx$$

$$K_{44} = \int_0^L \left[A_{44}\frac{d^2X_m}{dx^2}X_m - A_{55}X_m^2\right]dx$$

Appendix B. Supplementary data

Supplementary data to this article can be found online at https://doi.org/10.1016/j.compstruct.2020.112486.

References

[1] Koizumi M. FGM activities in Japan. Compos B 1997;28:1–4.
[2] Koizumi M, Niino M. Overview of FGM Research in Japan. MRS Bull 1995;20:19–21.
[3] Kayser WA, Ilschner B. FGM research activities in Europe. MRS Bull 1995;20:22–6.
[4] Sasaki M, Wang Y, Hirano T, Hirai T. Design of SiC/C functionally gradient material and its preparation by chemical vapor deposition. J Ceram Soc Jpn 1989;97:539–43.
[5] Miyamoto Y, Kaysser WA, Rabin BH, Kawasaki A, Ford RG. Functionally Graded Materials: Design, Processing and Applications, Springer, Springer Science & Business. Media 2013;5:1–317.
[6] Timoshenko SP. On the correction for shear of the differential equation for transverse vibrations of prismatic bars. The London, Edinburgh, and Dublin Philosophical Magazine and Journal of Science 1921;41:744–6.
[7] Reddy JN. A simple higher-order theory for laminated composite plates. J Appl Mech 1984;45:745–52.
[8] Akavci SS, Tanrikulu AH. Static and free vibration analysis of functionally graded plates based on a new quasi-3D and 2D shear deformation theories. Compos B 2015;83:203–15.
[9] Vo ThP, Thai H-T, Nguyen T-K, Inam F, Lee J. A quasi-3D theory for vibration and buckling of functionally graded sandwich beams. Compos Struct 2015;119:1–12.
[10] Do VNV, Lee C-H. Quasi-3D higher-order shear deformation theory for thermal buckling analysis of FGM plates based on a meshless method. Aerosp Sci Technol 2018;82–83:450–65.
[11] Shahsavari D, Shahsavari M, Li L, Karami B. A novel quasi-3D hyperbolic theory for free vibration of FG plates with porosities resting on Winkler/Pasternak/Kerr foundation. Aerosp Sci Technol 2018;72:134–49.
[12] Zohra Zaoui F, Ouinas D, Tounsi A. New 2D and quasi-3D shear deformation theories for free vibration of functionally graded plates on elastic foundations. Compos B Eng 2019;159:231–47.
[13] Kiani Y, Eslami MR. Thermal buckling analysis of functionally graded material beams. Int J Mech Mater Des 2010;6:229–38.
[14] Wattanasakulpong N, Gangadhara Prusty B, Kelly DW. Thermal buckling and elastic vibration of third-order shear deformable functionally graded beams. Int J Mech Sci 2011;53:734–43.
[15] Fallah A, Aghdam MM. Thermo-mechanical buckling and nonlinear free vibration analysis of functionally graded beams on nonlinear elastic foundation. Compos B 2012;43:1523–30.
[16] Ma LS, Lee DW. Exact solutions for nonlinear static responses of a shear deformable FGM beam under an in-plane thermal loading. Eur J Mech A Solids 2012;31:13–20.
[17] Rahimi GH, Gazor MS, Hemmatnezhad M, Toorani H. On the postbuckling and free vibrations of FG Timoshenko beams. Compos Struct 2013;95:247–53.
[18] Esfahani SE, Kiani Y, Eslami MR. Non-linear thermal stability analysis of temperature dependent FGM beams supported on non-linear hardening elastic foundations. Int J Mech Sci 2013;69:10–20.
[19] Viola E, Tornabene F, Fantuzzi N. General higher-order shear deformation theories for the free vibration analysis of completely doubly-curved laminated shells and panels. Compos Struct 2013;95:639–66.
[20] Viola E, Tornabene F, Fantuzzi N. Static analysis of completely doubly-curved laminated shells and panels using general higher-order shear deformation theories. Compos Struct 2013;101:59–93.
[21] Tornabene F, Viola E, Fantuzzi N. General higher-order equivalent single layer theory for free vibrations of doubly-curved laminated composite shells and panels. Compos Struct 2013;104:94–117.
[22] Vo ThP, Thai H-T, Nguyen T-K, Maheri A, Lee J. Finite element model for vibration and buckling of functionally graded sandwich beams based on a refined shear deformation theory. Eng Struct 2014;64:12–22.
[23] Tornabene F, Fantuzzi N, Viola E, Ferreira AJM. Radial basis function method applied to doubly-curved laminated composite shells and panels with a General Higher-order Equivalent Single Layer formulation. Compos B 2013;55:642–59.
[24] Shen H-Sh, Wang Zh-X. Nonlinear analysis of shear deformable FGM beams resting on elastic foundations in thermal environments. Int J Mech Sci 2014;81:195–206.
[25] Tornabene F, Fantuzzi N, Bacciocchi M. The local GDQ method applied to general higher-order theories of doubly-curved laminated composite shells and panels: The free vibration analysis. Compos Struct 2014;116:637–60.
[26] Nguyen T-K, Truong-Phong Nguyen T, Vo ThP, Thai H-T. Vibration and buckling analysis of functionally graded sandwich beams by a new higher-order shear deformation theory. Compos B Eng 2015;76:273–85.
[27] Tufeksi E, Eroglu U, Aydin S. Aya, Exact solution for in-plane static problems of circular beams made of functionally graded materials, Mechanics Based Design of Structures and Machines An. International Journal 2016;44:476–94.
[28] Chen D, Yang J, Kitipornchai S. Elastic buckling and static bending of shear deformable functionally graded porous beam. Compos Struct 2015;133:54–61.
[29] Simsek M. Buckling of Timoshenko beams composed of two-dimensional functionally graded material (2D-FGM) having different boundary conditions. Compos Struct 2016;149:304–14.
[30] Huang Y, Zhang M, Rong H. Buckling Analysis of Axially Functionally Graded and Non-Uniform Beams Based on Timoshenko Theory. Acta Mech Solida Sin 2016;29:200–7.
[31] She G-L, Yuan F-G, Ren Y-R. Thermal buckling and post-buckling analysis of functionally graded beams based on a general higher-order shear deformation theory. Appl Math Model 2017;47:340–57.
[32] Kahya V, Turan M. Finite element model for vibration and buckling of functionally graded beams based on the first-order shear deformation theory. Compos B 2017;109:108e115.
[33] Deng H, Dong Chen K, Cheng W, Zhao ShG. Vibration and buckling analysis of double-functionally graded Timoshenko beam system on Winkler-Pasternak elastic foundation. Compos Struct 2017;160:152–68.
[34] Sina SA, Navazi HM, Haddadpour H. An analytical method for free vibration analysis of functionally graded beams. Mater Des 2009;30:741–7.
[35] Ke L-L, Yang J, Kitipornchai S. An analytical study on the nonlinear vibration of functionally graded beams. Meccanica 2010;45:743–52.
[36] Hein H, Feklistova L. Free vibrations of non-uniform and axially functionally graded beams using Haar wavelets. Eng Struct 2011;33:3696–701.
[37] Shooshtari A, Rafiee M. Nonlinear forced vibration analysis of clamped functionally graded beams. Acta Mech 2011;221:23–38.
[38] Wattanasakulpong N, Gangadhara Prusty B, Kelly DW, Hoffman M. Free vibration analysis of layered functionally graded beams with experimental validation. Mater Des 2012;36:182–90.
[39] Thai H-Tai, Vo ThP. Bending and free vibration of functionally graded beams using various higher-order shear deformation beam theories. Int J Mech Sci 2012;62:57–66.
[40] Pradhan KK, Chakraverty S. Free vibration of Euler and Timoshenko functionally graded beams by Rayleigh-Ritz method. Compos B 2013;51:175–84.
[41] Kanani AS, Niknam H, Ohadi AR, Aghdam MM. Effect of nonlinear elastic foundation on large amplitude free and forced vibration of functionally graded beam. Compos Struct 2014;115:60–8.
[42] Su H, Banerjee JR. Development of dynamic stiffness method for free vibration of functionally graded Timoshenko beams. Comput Struct 2015;147:107–16.
[43] Tossapanon P, Wattanasakulpong N. Stability and free vibration of functionally graded sandwich beams resting on two-parameter elastic foundation. Compos Struct 2016;142:215–25.
[44] Chen D, Yang J, Kitipornchai S. Free and forced vibrations of shear deformable functionally graded porous beams. Int J Mech Sci 2016;108–109:14–22.
[45] Jing L-L, Ming P-J, Zhang W-P, Fu L-R, Cao Y-P. Static and free vibration analysis of functionally graded beams by combination Timoshenko theory and finite volume method. Compos Struct 2016;138:192–213.
[46] Paul A, Das D. Free vibration analysis of pre-stressed FGM Timoshenko beams under large transverse deflection by a variational method. Engineering Science and Technology, an International Journal 2016;19:1003–17.
[47] Wang X. Shirong Li, Free vibration analysis of functionally graded material beams based on Levinson beam theory. Applied Mathematics and Mechanics (English Edition) 2016;37:861–78.
[48] Nguyen DK, Nguyen QH, Tran TT, Bui VT. Vibration of bi-dimensional functionally graded Timoshenko beams excited by a moving load. Acta Mech 2017;228:141–55.
[49] Celebi K, Yarimpabuc D, Tutuncu N. Free vibration analysis of functionally graded beams using complementary functions method. Arch Appl Mech 2018;88:729–39.
[50] Sinir S, Çevik M, Gültekin Sinir B. Nonlinear free and forced vibration analyses of axially functionally graded Euler-Bernoulli beams with non-uniform cross-section. Compos B Eng 2018;148:123–31.
[51] Banerjee JR, Ananthapuvirajah A. Free vibration of functionally graded beams and frameworks using the dynamic stiffness method. J Sound Vib 2018;422:34–47.
[52] Karamanli A. Free vibration analysis of two directional functionally graded beams using a third order shear deformation theory. Compos Struct 2018;189:127–36.
[53] Fazzolari FA. Generalized exponential, polynomial and trigonometric theories for vibration and stability analysis of porous FG sandwich beams resting on elastic foundations. Compos B Eng 2018;136:254–71.
[54] Cao D, Gao Y. Free vibration of non-uniform axially functionally graded beams using the asymptotic development method. Appl Math Mech 2019;40:85–96.
[55] Arefi M, Pourjamshidian M, Ghorbanpour Arani A, Rabczuk T. Influence of flexoelectric, small-scale, surface and residual stress on the nonlinear vibration of sigmoid, exponential and power-law FG Timoshenko nano-beams, Journal of Low Frequency Noise, Vibration and Active. Control 2019;38:122–42.
[56] Almitani KhH. Buckling Behaviors of Symmetric and Antisymmetric Functionally Graded Beams. Journal of Applied and Computational Mechanics 2018;4:115–24.

[57] Ramirez D, Cuba L, Mantari JL, Arciniega RA. Bending and Free Vibration Analysis of Functionally Graded Plates via Optimized Non-polynomial Higher Order Theories. Journal of Applied and Computational Mechanics 2019;5:281–98.
[58] Sayyad A, Ghumare Sh. A New Quasi-3D Model for Functionally Graded Plates. Journal of Applied and Computational Mechanics 2019;5:367–80.
[59] Doğuşcan Akbaş Ş. Hygro-Thermal Nonlinear Analysis of a Functionally Graded Beam. Journal of Applied and Computational Mechanics 2019;5:477–85.
[60] Esmaeili M, Tadi Beni Y. Vibration and Buckling Analysis of Functionally Graded Flexoelectric Smart Beam. Journal of Applied and Computational Mechanics 2019;5:900–17.
[61] Bîrsan M, Altenbach H, Sadowski T, Eremeyev VA, Pietras D. Deformation analysis of functionally graded beams by the direct approach. Compos B Eng 2012;43:1315–28.
[62] Altenbach H, Eremeyev VA. On the Time-Dependent Behavior of FGM Plates. Key Eng Mater 2008;399:63–70.
[63] Yang Y-F, Chen D, Yang B. 3D thermally induced analysis of annular plates of functionally graded materials. Theor Appl Mech Lett 2019;9:297–301.
[64] Kumar Jena S, Chakraverty S, Malikan M. Application of shifted Chebyshev polynomial-based Rayleigh-Ritz method and Navier's technique for vibration analysis of a functionally graded porous beam embedded in Kerr foundation. Engineering with Computers 2020. https://doi.org/10.1007/s00366-020-01018-7.
[65] Atmane HA, Tounsi A, Bernard F. Effect of thickness stretching and porosity on mechanical response of a functionally graded beams resting on elastic foundations. Int J Mech Mater Des 2017;13:71–84.
[66] Dastjerdi Sh, Akgöz B. New static and dynamic analyses of macro and nano FGM plates using exact three-dimensional elasticity in thermal environment. Compos Struct 2018;192:626–41.
[67] Naebe M, Shirvanimoghaddam K. Functionally graded materials: A review of fabrication and properties. Appl Mater Today 2016;5:223–45.
[68] Czechowski L, Kołakowski Z. Analysis of the functionality step-variable graded plate under in-plane compression. Materials 2019;12:4090.
[69] Malikan M, Tornabene F, Dimitri R. Nonlocal three-dimensional theory of elasticity for buckling behavior of functionally graded porous nanoplates using volume integrals. Mater Res Express 2018;5:095006.
[70] Karami B, Shahsavari D, Janghorban M, Li L. On the resonance of functionally graded nanoplates using bi-Helmholtz nonlocal strain gradient theory. Int J Eng Sci 2019;144:103143.
[71] Zharfi H. Creep relaxation in FGM rotating disc with nonlinear axisymmetric distribution of heterogeneity. Theor Appl Mech Lett 2019;9:382–90.
[72] Zenkour AM. A simple four-unknown refined theory for bending analysis of functionally graded plates. Appl Math Model 2013;37:9041–51.
[73] Touratier M. An efficient standard plate theory. Int J Eng Sci 1991;29:901–16.
[74] Mantari J, Oktem A, Soares CG. A new trigonometric shear deformation theory for isotropic, laminated composite and sandwich plates. Int J Solids Struct 2012;49:43–53.
[75] Joshan YS, Santapuri S. Neeraj Grover, Analysis of laminated piezoelectric composite plates using an inverse hyperbolic coupled plate theory. Appl Math Model 2020;82:359–78.
[76] Neves AMA, Ferreira AJM, Carrera E, Roque CMC, Cinefra M, Jorge RMN, et al. A quasi-3D sinusoidal shear deformation theory for the static and free vibration analysis of functionally graded plates. Compos B 2012;43:711–25.
[77] Neves AMA, Ferreira AJM, Carrera E, Roque CMC, Cinefra M, Jorge RMN, et al. A quasi-3D hyperbolic shear deformation theory for the static and free vibration analysis of functionally graded plates. Compos Struct 2012;94:1814–25.
[78] Sarangan S, Singh BN. Higher-order closed-form solution for the analysis of laminated composite and sandwich plates based on new shear deformation theories. Compos Struct 2016;138:391–403.
[79] Aydogdu M. A new shear deformation theory for laminated composite plates. Compos Struct 2009;89:94–101.
[80] Soldatos KP. A transverse shear deformation theory for homogeneous monoclinic plates. Acta Mech 1992;94:195–220.
[81] Karama M, Afaq KS, Mistou S. A new theory for laminated composite plates. Journal of Materials Design and Applications 2009;223:53–62.
[82] Thai HT, Choi DH. Improved refined plate theory accounting for effect of thickness stretching in functionally graded plates. Compos B 2014;56:705–16.
[83] Hebali H, Tounsi A, Houari MSA, Bessaim A, Bedia EAA. New quasi-3D hyperbolic shear deformation theory for the static and free vibration analysis of functionally graded plates. J Eng Mech 2014;140:374–83.
[84] Avcar M. Elastic buckling of steel columns under axial compression. American Journal of Civil Engineering 2014;2:102–8.
[85] Fan Q, Chai Ch, Wei Q, Yang Y. The Mechanical and Electronic Properties of Carbon-Rich Silicon Carbide. Materials 2016;9:333.
[86] Zidi M, Tounsi A, Houari MSA, Adda Bedia EA, Bég OA. Bending analysis of FGM plates under hygro-thermo-mechanical loading using a four variable refined plate theory. Aerosp Sci Technol 2014;34:24–34.
[87] Yang J, Shen H-S. Vibration characteristics and transient response of shear-deformable functionally graded plates in thermal environments. J Sound Vib 2002;255:579–602.
[88] Reddy JN, Chin CD. Thermo-mechanical analysis of functionally graded cylinders and plates. J Therm Stresses 1998;21:593–626.